PROCEEDINGS OF SCIENCE

Angular analyses of $b \to s\mu^+\mu^-$ transitions at CMS

Dayong Wang[*†]
for the CMS Collaboration

State Key Laboratory of Nuclear Physics and Technology, Peking University, Beijing, China
E-mail: dayong.wang@pku.edu.cn

The flavour changing neutral current decays can be interesting probes for searching for new physics. Angular distributions of $b \to s\ell^+\ell^-$ transition processes of both $B^0 \to K^{*0}\mu^+\mu^-$ and $B^+ \to K^+\mu^+\mu^-$ are studied using a sample of proton-proton collisions at $\sqrt{s} = 8$ TeV collected with the CMS detector at the LHC, corresponding to an integrated luminosity of 20.5 fb^{-1}. Angular analyses are performed to determine P_1 and P_5' angular parameters for $B^0 \to K^{*0}\mu^+\mu^-$ and A_{FB} and F_H parameters for $B^+ \to K^+\mu^+\mu^-$, all as functions of the dimuon invariant mass squared. The P_5' parameter is of particular interest due to recent measurements that indicate a potential discrepancy with the standard model. All the measurements are consistent with the standard model predictions. Efforts with more channels and more coming data will be continued to further test the standard model with higher precision in future.

The International Conference on B-Physics at Frontier Machines - BEAUTY2018
6-11 May, 2018
La Biodola, Elba Island, Italy

[*]Speaker.
[†]Partially supported by the Ministry of Science and Technology of China, under Grants No. 2013CB837800.

PoS(BEAUTY2018)045

1. Introduction

The Compact Muon Solenoid (CMS) at CERN [1] is a general-purpose detector currently running on the large hadron collider (LHC). It is equipped with large area of silicon trackers, a 3.8T magnetic field, superb muon detection systems with large acceptance and very flexible trigger systems. These features make CMS an ideal detector for performing precise measurements of heavy flavor physics.

Phenomena beyond the standard model (SM) of particle physics can become manifest directly, via the production of new particles, or indirectly, by affecting the production and decay of SM particles. The transitions of the type $b \to s\ell^+\ell^-$ is a flavor-changing neutral current (FCNC) process, with ℓ denoting a charged lepton. In the SM, this type of transition is forbidden at tree level and occurs through higher-order processes via either electroweak Z/γ penguin diagrams or a W^+W^- box diagram, as shown in Fig. 1. This makes the measurement of these rare FCNC decays more sensitive to possible physics phenomena beyond the SM (BSM).

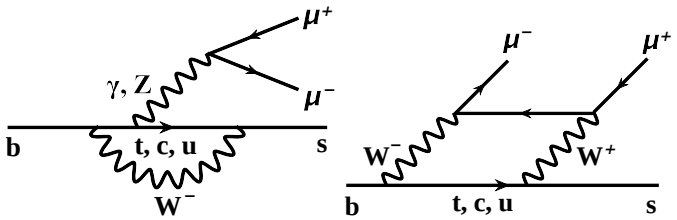

Figure 1: The SM electroweak penguin (Left) and box (Right) diagrams for the transition $b \to s\ell^+\ell^-$.

CMS has recently analysed two such FCNC decays: $B^0 \to K^{*0}\mu^+\mu^-$, where K^{*0} indicates the $K^{*0}(892)$ meson, and $B^+ \to K^+\mu^+\mu^-$. Both analyses use a sample of events collected in proton-proton (pp) collisions at a center-of-mass energy of 8 TeV with the CMS detector at LHC. The data correspond to an integrated luminosity of 20.5 fb^{-1} [2]. The data for these analysis was recorded using a low-mass dimuon HLT with a displaced vertex.

2. Angular analysis of $B^0 \to K^{*0}\mu^+\mu^-$ [3]

The differential decay rate for $B^0 \to K^{*0}\mu^+\mu^-$ can be written in terms of the dimuon mass squared (q^2) and three angular variables as a combination of spherical harmonics. Figure 2 shows the angular variables defining the decay kinematics: θ_ℓ is the angle between the positive (negative) muon momentum and the direction opposite to the B^0 ($\bar{B^0}$) in the dimuon rest frame, θ_K is the angle between the kaon momentum and the direction opposite to the B^0 ($\bar{B^0}$) in the K^{*0} ($\bar{K^{*0}}$) rest frame, and φ is the angle between the plane containing the two muons and the plane containing the kaon and pion in the B^0 rest frame.

New physics may modify any of the angular variables [4] relative to their SM values[5, 6]. Previous measurements of some of these quantities by the BaBar, Belle, CDF, LHCb, and CMS experiments are consistent with the SM[7]. The P_5' parameter in the decay $B^0 \to K^{*0}\mu^+\mu^-$ is of particular interest due to recent LHCb and Belle measurements [8, 9, 10] that indicate a potential discrepancy with the standard model. CMS performed a new measurement of the P_1 and P_5' angular parameters [3], trying to elucidate the situation. In the measurement, the values of P_1 and P_5' angular

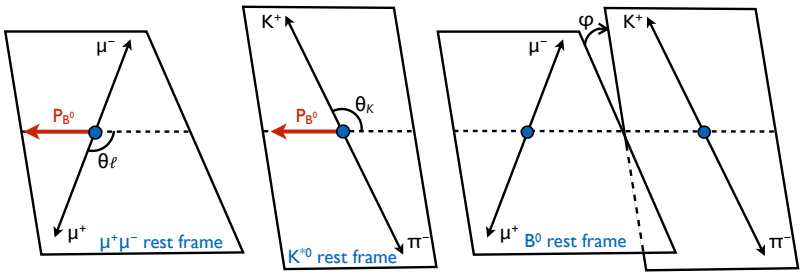

Figure 2: Sketch showing the definition of the angular variables θ_ℓ (left), θ_K (middle), and φ (right) for the decay $B^0 \to K^{*0}\mu^+\mu^-$.

parameters are determined by fitting the distribution of events as a function of the three angular variables. All measurements are performed in q^2 bins from 1 to 19 GeV^2. The q^2 bins $8.68 < q^2 < 10.09$ GeV^2 and $12.90 < q^2 < 14.18$ GeV^2, corresponding to $B^0 \to K^{*0}J/\psi$ and $B^0 \to K^{*0}\psi'$ decays, respectively, are used to validate the analysis.

There can be a contribution from spinless (S-wave) $K^-\pi^+$ combinations [6]. This is parametrized with three terms: F_S, which is related to the S-wave fraction, and A_S and A_S^5, which are the interference amplitudes between the S-wave and P-wave decays. Including these components, the angular distribution of $B^0 \to K^{*0}\mu^+\mu^-$ can be written as [6]:

$$\begin{aligned}\frac{1}{\mathrm{d}\Gamma/\mathrm{d}q^2}\frac{\mathrm{d}^4\Gamma}{\mathrm{d}q^2\mathrm{d}\cos\theta_\ell\mathrm{d}\cos\theta_K\mathrm{d}\varphi} = \frac{9}{8\pi}\Bigg\{&\frac{2}{3}\Big[(F_S + A_S\cos\theta_K)\left(1-\cos^2\theta_\ell\right) + A_S^5\sqrt{1-\cos^2\theta_K}\\ &\sqrt{1-\cos^2\theta_\ell}\cos\varphi\Big] + (1-F_S)\Big[2F_L\cos^2\theta_K\left(1-\cos^2\theta_\ell\right)\\ &+\frac{1}{2}(1-F_L)\left(1-\cos^2\theta_K\right)\left(1+\cos^2\theta_\ell\right) + \frac{1}{2}P_1(1-F_L)\\ &(1-\cos^2\theta_K)(1-\cos^2\theta_\ell)\cos 2\varphi + 2P_5'\cos\theta_K\sqrt{F_L(1-F_L)}\\ &\sqrt{1-\cos^2\theta_K}\sqrt{1-\cos^2\theta_\ell}\cos\varphi\Big]\Bigg\}.\end{aligned} \tag{2.1}$$

where F_L denotes the longitudinal polarization fraction of the K^{*0}. This expression is an exact simplification of the full angular distribution, obtained by folding the φ and θ_ℓ angles about zero and $\pi/2$, respectively.

For each q^2 bin, the observables of interest are extracted from an unbinned extended maximum-likelihood fit to four variables: the $K^+\pi^-\mu^+\mu^-$ invariant mass m and the three angular variables θ_ℓ, θ_K, and φ. For each q^2 bin, the unnormalized probability density function (pdf) has the following expression:

$$\begin{aligned}\mathrm{pdf}(m,\theta_K,\theta_\ell,\varphi) = Y_S^C\Big[&S^C(m)\,S^a(\theta_K,\theta_\ell,\varphi)\,\varepsilon^C(\theta_K,\theta_\ell,\varphi)\\ &+\frac{f^M}{1-f^M}\,S^M(m)\,S^a(-\theta_K,-\theta_\ell,\varphi)\,\varepsilon^M(\theta_K,\theta_\ell,\varphi)\Big]\\ &+Y_B\,B^m(m)\,B^{\theta_K}(\theta_K)\,B^{\theta_\ell}(\theta_\ell)\,B^{\varphi}(\varphi),\end{aligned} \tag{2.2}$$

where the contributions correspond to correctly tagged signal events, mistagged signal events, and background events. The parameters Y_S^C and Y_B are the yields of correctly tagged signal events and background events, respectively, and are free parameters in the fit. The parameter f^M is the fraction of signal events that are mistagged and is determined from MC simulation. The signal mass probability functions $S^C(m)$ and $S^M(m)$ are each the sum of two Gaussian functions sharing the same mean, and describe the mass distribution for correctly tagged and mistagged signal events, respectively.

In the fit, the mean, the four Gaussian σ parameters, and two fractions relating the contribution of each Gaussian, are determined from simulation, which has been found to accurately reproduce the data. The function $S^q(\theta_K, \theta_\ell, \varphi)$ describes the signal in the three-dimensional (3D) space of the angular variables and corresponds to Eq. (2.1). The combination $B^m(m)\,B^{\theta_K}(\theta_K)\,B^{\theta_\ell}(\theta_\ell)\,B^{\varphi}(\varphi)$ is obtained from B^0 sideband data and describes the background in the space of $(m, \theta_K, \theta_\ell, \varphi)$, where the mass distribution is an exponential function and the angular distributions are polynomials ranging from second to fourth degree, for both $B^{\theta_K}(\theta_K)$ and $B^{\theta_\ell}(\theta_\ell)$, depending on the q^2 bin, while the term $B^{\varphi}(\varphi)$ is of first degree for all q^2 bins. The functions $\varepsilon^C(\theta_K, \theta_\ell, \varphi)$ and $\varepsilon^M(\theta_K, \theta_\ell, \varphi)$ are the efficiencies in the 3D space of $-1 \leq \cos\theta_K \leq 1, 0 \leq \cos\theta_\ell \leq 1$, and $0 \leq \varphi \leq \pi$ for correctly tagged and mistagged signal events, respectively.

The fit is performed in two steps. The initial fit uses the data from the sidebands of the B^0 mass to obtain the $B^m(m)$, $B^{\theta_K}(\theta_K)$, $B^{\theta_\ell}(\theta_\ell)$, and $B^{\varphi}(\varphi)$ distributions (the signal component is absent from this fit). The sideband regions are $3\sigma_m < |m - m_{\mathrm{B}^0}| < 5.5\sigma_m$, where σ_m is the average mass resolution ($\approx$45MeV), obtained from fitting the MC simulation signal to a sum of two Gaussians with a common mean. The distributions obtained in this step are then fixed for the second step, which is a fit to the data over the full mass range. The free parameters in this fit are the angular parameters P_1, P_5', and A_{S}^5, and the yields Y_S^C and Y_B. In the fits, the angular parameters F_{L}, F_{S}, and A_{S} are fixed to previous CMS measurements performed on the same data set with the same event selection criteria [7].

Table 1: Systematic uncertainties in P_1 and P_5'. For each source, the range indicates the variation over the bins in q^2.

Source	$P_1(\times 10^{-3})$	$P_5'(\times 10^{-3})$
Simulation mismodeling	1–33	10–23
Fit bias	5–78	10–120
Finite size of simulated samples	29–73	31–110
Efficiency	17–100	5–65
$K\pi$ mistagging	8–110	6–66
Background distribution	12–70	10–51
Mass distribution	12	19
Feed-through background	4–12	3–24
F_{L}, F_{S}, A_{S} uncertainty propagation	0–210	0–210
Angular resolution	2–68	0.1–12
Total	100–230	70–250

The fit formalism and results are validated through fits to pseudo-experimental samples, MC

simulation samples, and control channels. To ensure correct coverage for the uncertainties of the angular parameters, the Feldman-Cousins (FC) method [11] is used with nuisance parameters. The possible sources of systematic uncertainties investigated are summarized in Table 1. For the F_{L}, F_{S}, A_{S} uncertainty propagation, in the final fit, we fix the parameters, F_{L}, F_{S}, A_{S}, at the previous CMS measurements [7]. Their uncertainties are propagated to the final results.

The signal data, corresponding to 1397 events, are fit in seven q^2 bins from 1 to 19 GeV^2. As an example, distributions for the second q^2 bin, along with the fit projections, are shown in Fig. 3.

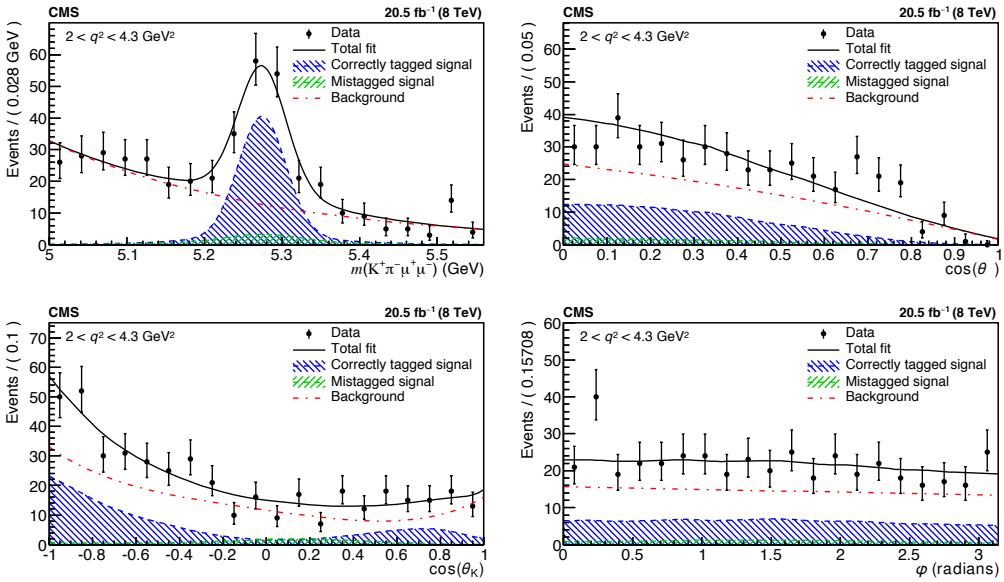

Figure 3: $\mathrm{K}^+\pi^-\mu^+\mu^-$ invariant mass and angular distributions for the second q^2 bin $2.00 < q^2 < 4.30$ GeV^2. Overlaid on each plot is the projection of the results for the total fit, as well as for the three components: correctly tagged signal, mistagged signal, and background. The vertical bars indicate the statistical uncertainties [3].

The fitted values of P_1, and P_5', along with their associated uncertainties, for each of the q^2 regions are shown in Fig. 4, along with the SM predictions. The results are among the most precise to date for these parameters and are consistent with predictions based on the standard model.

3. Angular analysis of $\mathrm{B}^+ \to \mathrm{K}^+\mu^+\mu^-$ [12]

The decay rate for the process $\mathrm{B}^+ \to \mathrm{K}^+\mu^+\mu^-$ depends on $\cos\theta_\ell$, where θ_ℓ is the angle between the directions of the μ^- and K^+ in the dilepton rest frame. The $\cos\theta_\ell$ dependence of the decay width Γ_ℓ can be parametrized [13, 14, 15] in terms of the observables of interest A_{FB} and F_{H} as:

$$\frac{1}{\Gamma_\ell}\frac{\Gamma_\ell}{\cos\theta_\ell} = \frac{3}{4}(1-F_{\mathrm{H}})(1-\cos^2\theta_\ell) + \frac{1}{2}F_{\mathrm{H}} + A_{\mathrm{FB}}\cos\theta_\ell. \tag{3.1}$$

The requirement for the decay rate to remain positive over all possible lepton angles constrains the parameter space to the region $0 \le F_{\mathrm{H}} \le 3$ and $|A_{\mathrm{FB}}| \le \min(1, F_{\mathrm{H}}/2)$.

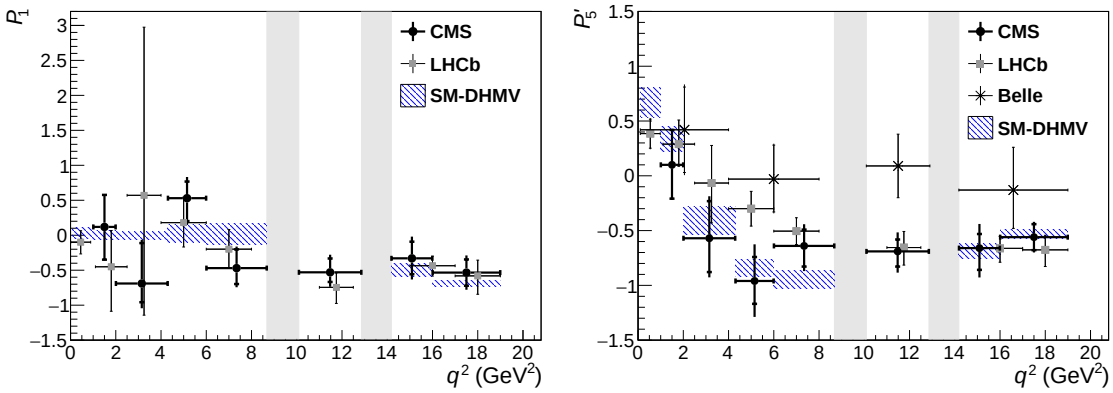

Figure 4: CMS measurements of the (left) P_1 and (right) P_5' angular parameters versus q^2 for $B^0 \to K^{*0}\mu^+\mu^-$ decays [3], in comparison to results from the LHCb [9] and Belle [10] Collaborations. The statistical uncertainties are shown by the inner vertical bars, while the outer vertical bars give the total uncertainties. The horizontal bars show the bin widths. The vertical shaded regions correspond to the J/ψ and ψ' resonances. The hatched region shows the prediction from SM calculations from Refs. [4, 6], averaged over each q^2 bin.

In the analysis, the selected events are reconstructed through the decay into the fully charged final state of one charged hadron and a pair of oppositely charged muons. Events from the control channels $B^+ \to K^+ J/\psi(\mu^+\mu^-)$ and $B^+ \to K^+ \psi'(\mu^+\mu^-)$ have the same final state as the signal process $B^+ \to K^+\mu^+\mu^-$. Dimuon candidates are formed from two oppositely charged muons matching the HLT criteria that triggered the event readout. To discriminate signal events from background, additional selection criteria on kinematic variables are used. These selection criteria are determined through a maximization of the expected signal significance using MC signal events and the surviving data events in the final B^+ meson invariant mass fitting region, 5.1–5.6 GeV. After applying the selection criteria, less than 10% of the selected events contain multiple B^+ candidates. In these events, only the candidate with the highest B^+ decay vertex fit probability is retained.

Events with a dimuon invariant mass (q) close to the J/ψ or ψ' resonance region are rejected to remove this contamination from the control channels. The J/ψ and ψ' resonance regions are defined as $m^{\rm PDG}_{J/\psi} - 5\sigma_q < q < m_{J/\psi} + 3\sigma_q$ and $|q - m^{\rm PDG}_{\psi'}| < 5\sigma_q$, respectively, where σ_q is the calculated uncertainty in q, and the PDG superscript indicates the world-average mass value [16] for each particle. We further suppress such events by requiring, $|(m - m^{\rm PDG}_{B^+}) - (q - m^{\rm PDG}_{J/\psi})| > 0.13$ GeV and $|(m - m^{\rm PDG}_{B^+}) - (q - m^{\rm PDG}_{\psi'})| > 0.06$ GeV in the B^+ meson invariant mass region of 5.1–5.6 GeV.

MC simulated event samples are widely used in the analysis. The number of simulated events for the signal sample $B^+ \to K^+\mu^+\mu^-$ corresponds to more than 160 times that of the data. The control channels for this analysis are $B^+ \to K^+ J/\psi(\mu^+\mu^-)$, $B^+ \to K^+ \psi'(\mu^+\mu^-)$, where the muon pairs come from J/ψ or ψ' decays.

The angular observables $A_{\rm FB}$ and $F_{\rm H}$ are extracted from a two-dimensional extended unbinned maximum-likelihood fit to the angular distribution of the selected B^+ meson candidates in each q^2 range. The unnormalized probability density function (pdf) used in the two-dimensional fit is:

$$\mathrm{pdf}(m, \cos\theta_\ell) = Y_{\rm S} \times S_{\rm m}(m) \times S_{\rm a}(\cos\theta_\ell) \times \varepsilon(\cos\theta_\ell) + Y_{\rm B} \times B_{\rm m}(m) \times B_{\rm a}(\cos\theta_\ell), \qquad (3.2)$$

where the two contributions on the righthand side correspond to the parametrization of the signal and background. The parameters Y_S and Y_B are the yields of signal and background events, respectively. The functions $S_m(m)$ and $S_a(\cos\theta_\ell)$ describe the signal invariant mass and angular distributions, while $B_m(m)$ and $B_a(\cos\theta_\ell)$ are similar functions describing the background. The function $\varepsilon(\cos\theta_\ell)$ is the signal efficiency as a function of $\cos\theta_\ell$.

The signal efficiency $\varepsilon(\cos\theta_\ell)$ is factorized into an acceptance ε_{acc} times a reconstruction efficiency ε_{reco}, which are both functions of $\cos\theta_\ell$. The signal efficiency $\varepsilon(\cos\theta_\ell)$ is parametrized and fit with a sixth-order polynomial for the nine different signal q^2 ranges used in this analysis. The signal distribution $S_m(m)$ is modeled as the sum of two Gaussian functions with a common mean, and $S_a(\cos\theta_\ell)$ is given in Eq. (3.1). The background distribution $B_m(m)$ is modeled as a single exponential function, while $B_a(\cos\theta_\ell)$ is parametrized as the sum of a Gaussian function and a third- or fourth-degree polynomial, depending on the particular q^2 range. Many of the parameters in the final fit are set to a given value with a Gaussian constraint that reflects the input uncertainty of the value. The free parameters of the fit are Y_S, Y_B, A_{FB}, and F_H, as well as the exponential decay parameter of $B_m(m)$.

To validate the efficiency description derived from simulation, we check that the ratio of the branching fractions of the two control channels is consistent with the world-average value [16] within their uncertainties. The MC simulation samples are used to validate the fitting procedure in each q^2 range.

Several sources of systematic uncertainties are considered in this analysis. All systematic uncertainties in the measured values of A_{FB} and F_H, and the total systematic uncertainties are summarized in Table 2.

Table 2: Absolute values of the uncertainty contributions in the measurement of A_{FB} and F_H. For each item, the range indicates the variation of the uncertainty in the signal q^2 bins.

Systematic uncertainty	A_{FB} $(\times 10^{-2})$	F_H $(\times 10^{-2})$
Finite size of MC samples	0.4–1.8	0.9–5.0
Efficiency description	0.1–1.5	0.1–7.8
Kinematic mismodeling	0.1–2.8	0.1–1.4
Background parametrization model	0.1–1.0	0.1–5.1
Angular resolution	0.1–1.7	0.1–3.3
Dimuon mass resolution	0.1–1.0	0.1–1.5
Fitting biases	0.1–3.2	0.4–25
Background distribution	0.1–7.2	0.1–29
Total systematic uncertainty	1.6–7.5	4.4–39

The final fit is performed over the full B^+ meson invariant mass range and results in 2286 ± 73 signal events with q^2 from 1 to 22 GeV^2. Projections of the fit results from data for the $K^+\mu^+\mu^-$ invariant mass and $\cos(\theta_\ell)$ distributions for the inclusive q^2 bin of 1–22 GeV^2 (excluding the resonance regions) are shown in Fig. 5. To evaluate the statistical uncertainties, the 68.3% confidence level intervals on A_{FB} and F_H are estimated using the profiled Feldman–Cousins technique [11]. The systematic and statistical uncertainties are added in quadrature to obtain the total uncertainty.

The measured values of A_{FB} and F_H for each q^2 range are shown in Fig. 6. The measured val-

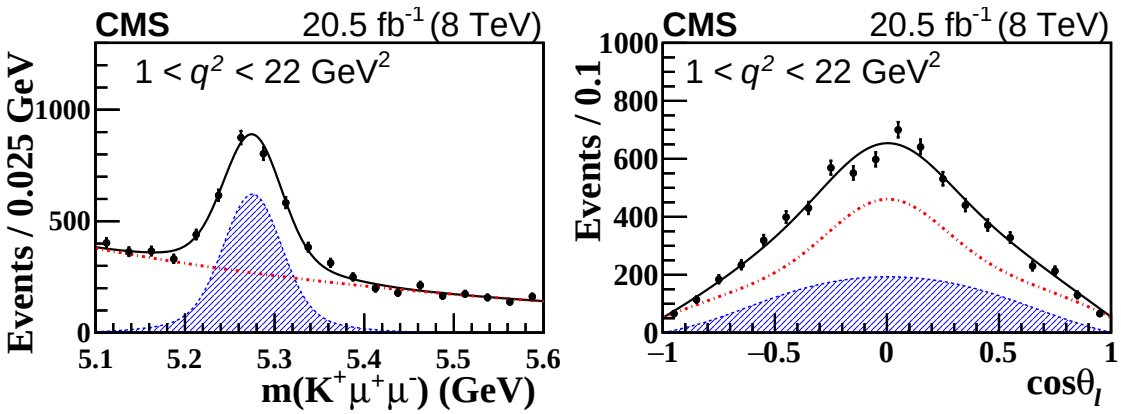

Figure 5: Projections of the fit results from data for the $K^+\mu^+\mu^-$ invariant mass and $\cos(\theta_\ell)$ distributions for the inclusive q^2 bin of 1–22 GeV^2 (excluding the resonance regions). The vertical bars represent the statistical uncertainties in the data [12].

ues of $A_{\rm FB}$ are consistent with the SM expectation of no asymmetry. We also compare the measured results with three SM predictions for $F_{\rm H}$ with different input parameters and different handling of higher-order corrections, one of which is also shown in Fig. 6. There is generally good agreement between the predictions and our results, as well as between our results and previous measurements [19, 20, 21, 22, 23].

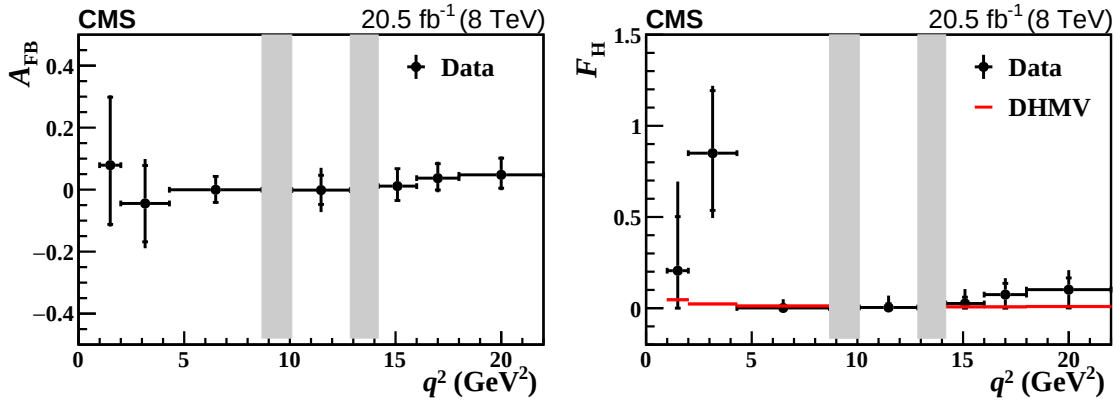

Figure 6: Results of the measurement of $A_{\rm FB}$ (left) and $F_{\rm H}$ (right) in bins of q^2 [12]. The statistical uncertainties are shown by the inner vertical bars, while the outer vertical bars give the total uncertainties. The horizontal bars show the bin widths. The vertical shaded regions are 8.68–10.09 and 12.86–14.18 GeV^2, and correspond to the J/ψ and ψ'-dominated control regions, respectively. The red line in the right plot shows the DHMV SM theoretical prediction [17, 18].

4. Summary and outlook

Using pp collision data recorded at $\sqrt{s} = 8$ TeV with the CMS detector at the LHC, corresponding to an integrated luminosity of 20.5 fb^{-1}, angular analyses have been performed for the

decays of $B^0 \to K^{*0}\mu^+\mu^-$ and $B^+ \to K^+\mu^+\mu^-$. For each bin of the dimuon invariant mass squared (q^2), unbinned maximum-likelihood fits were performed to the distributions of the B meson invariant mass and the three decay angles, to obtain values of angular parameters. The results are among the most precise to date and are consistent with previous measurements and with standard model predictions. CMS efforts with more channels and more coming data will be continued to further test the standard model with higher precision in future.

References

[1] CMS Collaboration, S. Chatrchyan *et al.*, JINST **3**, S08004 (2008).

[2] CMS Collaboration, Report No. CMS–PAS–LUM–13–001, 2013. http://cdsweb.cern.ch/record/1598864

[3] CMS, A. M. Sirunyan *et al.*, Phys. Lett. **B781**, 517 (2018).

[4] S. Descotes-Genon, J. Matias, M. Ramon, and J. Virto, JHEP **01**, 048 (2013).

[5] S. Jäger and J. Martin Camalich, JHEP **05**, 043 (2013).

[6] S. Descotes-Genon, T. Hurth, J. Matias, and J. Virto, JHEP **05**, 137 (2013).

[7] CMS Collaboration, S. Chatrchyan *et al.*, Phys. Lett. B **753**, 424 (2016).

[8] LHCb Collaboration, R. Aaij *et al.*, Phys. Rev. Lett. **111**, 191801 (2013).

[9] LHCb Collaboration, R. Aaij *et al.*, JHEP **02**, 104 (2016).

[10] Belle Collaboration, A. Abdesselam *et al.*, Phys. Rev. Lett. **118**, 111801 (2017).

[11] G. J. Feldman and R. D. Cousins, Phys. Rev. D **57**, 3873 (1998).

[12] CMS Collaboration, A. M. Sirunyan *et al.*, arxiv:1806.00636, CERN–EP–2018–125,2018.

[13] C. Bobeth, G. Hiller, and G. Piranishvili, JHEP **12**, 040 (2007).

[14] A. Ali, P. Ball, L. T. Handoko, and G. Hiller, Phys. Rev. D **61**, 074024 (2000).

[15] C. Bobeth, T. Ewerth, F. Kruger, and J. Urban, Phys. Rev. D **64**, 074014 (2001).

[16] Particle Data Group, C. Patrignani *et al.*, Chin. Phys. C **40**, 100001 (2016).

[17] S. Descotes-Genon, L. Hofer, J. Matias, and J. Virto, JHEP **12**, 125 (2014).

[18] S. Descotes-Genon, L. Hofer, J. Matias, and J. Virto, JHEP **06**, 092 (2016).

[19] BABAR Collaboration, B. Aubert *et al.*, Phys. Rev. D **73**, 092001 (2006).

[20] Belle Collaboration, J.-T. Wei *et al.*, Phys. Rev. Lett. **103**, 171801 (2009).

[21] CDF Collaboration, T. Aaltonen *et al.*, Phys. Rev. Lett. **108**, 081807 (2012).

[22] LHCb Collaboration, R. Aaij *et al.*, JHEP **02**, 105 (2013).

[23] LHCb Collaboration, R. Aaij *et al.*, JHEP **05**, 082 (2014).